Contribution due to clumpy winds to the non-thermal emission in microquasar jets

V. M. de la Cita[1] **S. del Palacio**[2,3] **V. Bosch-Ramon**[1] **X. Paredes-Fortuny**[1] **G. E. Romero**[2,3]**, and D. Khangulyan**[4]

[1] Departament d'Astronomia i Meteorologia, Institut de Ciènces del Cosmos (ICCUB), Universitat de Barcelona (IEEC-UB), Martí i Franquès 1, E-08028 Barcelona, Spain
[2]Instituto Argentino de Radioastronomía (CCT La Plata, CONICET), C.C.5, (1894) Villa Elisa, Buenos Aires, Argentina.
[3]Facultad de Ciencias Astronómicas y Geofísicas, Universidad Nacional de La Plata, Paseo del Bosque, B1900FWA La Plata, Argentina.
[4]Department of Physics, Rikkyo University 3-34-1, Nishi-Ikebukuro, Toshima-ku, Tokyo 171-8501, Japan

Abstract

Powerful jets in high-mass microquasars are likely to be crossed by dense inhomogeneities (clumps) from the stellar winds, which may lead to particle acceleration and thus non-thermal emission in X-rays and gamma-rays. We characterise a typical clump-jet interaction scenario and compute the contribution to the high-energy emission of these systems. We use hydrodynamical simulations of a single clump-jet interaction and we use this result to compute its non-thermal (synchrotron and inverse Compton) radiation. We present several radiative calculations for a number of clump states, as the clump is disrupted over time, letting different parameters vary (viewing angle, magnetic field). We obtain significant amounts of non-thermal radiation from jet-clump interactions in high-mass microquasars.

1 Introduction

Jets are ubiquitous in the universe, and one of the best laboratories for particle acceleration and non-thermal radiation production at a wide range of scales. In particular, jets in microquasars are formed when the donor star transfers matter to the compact object companion, either a black hole or a neutron star; forming an accretion disk and the two opposite outflows. In this work we focus on high-mass microquasars (HMMQs), binary systems hosting a massive star (potentially with inhomogeneous winds, see e. g. [8]) and a compact object able to produce jets.
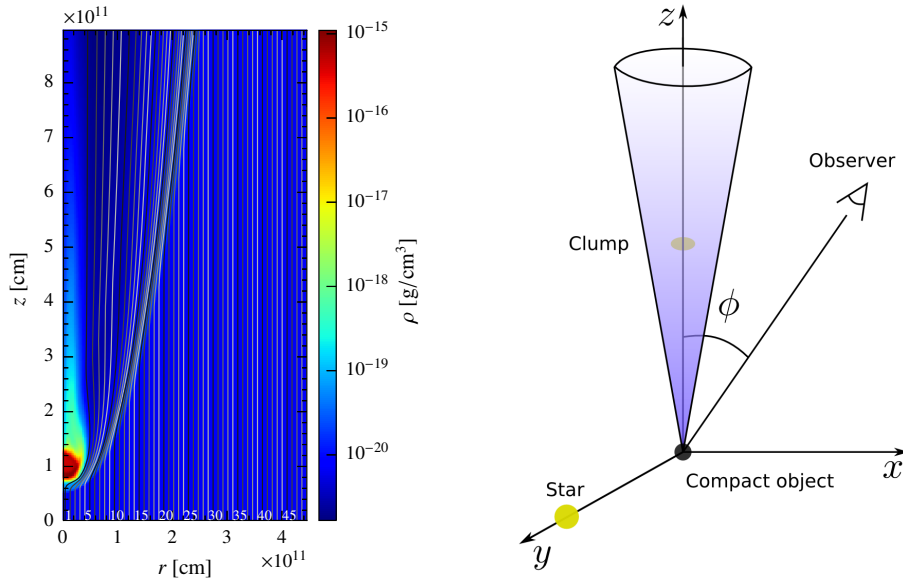
Figure 1: Left panel: Density map of the simulation, with the streamlines shown for illustrative purposes. Right panel: sketch of the hydrodynamic setup, defining the observer angle ϕ.

The importance of this clumps in the formation of shocks inside the jet is crucial, both in terms of its dynamical effect and its high-energy (HE) radiative output ([11, 9, 2, 10]). Up to date, the only two HMMQs detected in the GeV range are Cyg X-3 and Cyg X-1 (respectively, by [12, 13]), together with a 4.1σ flare-like detection of Cyg X-1 with the MAGIC Cherenkov telescope ([1]).

The work is structured as follows: in Sect. 2 we briefly resume the setup and how the simulations and the radiation computation are done; in Sect. 3 we present the radiative results with the specific focus on Cyg X-1 and Cyg X-3; and in Sect. 4 we discuss the GeV results coupled with the clump duty-cycle estimation, out of the scope of this text, but well described in [5], together with the application to Cyg X-1 and Cyg X-3.

2 Description of the setup and hydrodynamics

We performed relativistic hydrodynamic (RHD) simulations of the encounter of one of the microquasar jets with a stellar clump. We take advantage of the axi-symmetric nature of the system, making our simulations dimensional (2D), with the jet in the grid basis and the clump in the symmetry axis. The jet is considered perpendicular to the orbit and the clump is placed at a height with respect to the basis of the jet equal to the orbit separation R_{orb}. A simple sketch of the setup is shown in Fig. 1.

The clump is described by two factors: its radius R_c and its contrast density χ (the ratio between the density of the clump and the density of the rest of the wind). Taking

into account the inertia of the clumps one can infer the minimum radius necessary for a inhomogeneity to penetrate the jet, for a given jet opening angle θ_j:

$$R_{\rm c} > R_0 = 3 \times 10^{10} \left(\frac{\theta_{\rm j}}{0.1} \right) \left(\frac{10}{\chi} \right) \left(\frac{R_{\rm orb}}{3 \times 10^{12} \, {\rm cm}} \right) \, {\rm cm}. \tag{1}$$

Also, above certain jet luminosity ($L_{\rm j}$) threshold, the clump would be unable to enter the jet. We describe in [5] how do we get the relation between some stellar properties (wind speed $v_{\rm w}$, mass-loss rate $\dot{M}_{\rm w}$) and some jet parameters (speed, Lorentz factor and opening angle) to get the maximum jet luminosity for the jet to be penetrated by the clump:

$$L_{\rm j} \lesssim 1.4 \times 10^{37} \left(\frac{\Gamma_{\rm j} - 1}{\Gamma_{\rm j}} \right) \left(\frac{\chi}{10} \right) \left(\frac{\dot{M}_{\rm w}}{3 \times 10^{-6} M_\odot {\rm yr}^{-1}} \right) \left(\frac{\theta_{\rm j}}{0.1} \right)^2 \left(\frac{v_{\rm w}}{10^8 {\rm cm \, s}^{-1}} \right) \left(\frac{v_{\rm j}}{c} \right)^{-1} {\rm erg \, s}^{-1} \tag{2}$$

The RHD simulations were solved using the Marquina flux formula ([7, 6]). The hydrodynamic code is the same used in [3]. The resolution of the calculations is 300 cells in the vertical direction, the z-axis, and 150 in the radial direction, the r-axis, and the physical size is $z_{\rm grid}^{\rm max} = 9 \times 10^{11}$ cm in the z-direction, and $r_{\rm grid}^{\rm max} = 4.5 \times 10^{11}$ cm in the r-direction.

After running the RHD simulation we have to extract the streamlines, i.e. the fluid trajectories starting from several discrete positions in the base of the grid. How this streamlines are computed is described in [4], Appendix A, and is shown in Fig. 1.

We have simulated one single clump-jet interaction during ~ 820 s. During this time the clump creates a shock, expands, gets disrupted and eventually leaves the grid. We have focus on two main snapshots of this evolution: the stage in which spends the longer time (pictured in the color map in Fig. 1, referred to as *steady stage*) and a *flare stage* in which the shocked region is considerably large and, hence, the acceleration of electrons and their non-thermal output are also more important. It is important to notice that the magnetic field B does not enter in our hydrodynamic simulations, but it is imposed later as perpendicular to the fluid velocity and imposing that a fraction χ_B of the total flow energy flux is in the form of Poynting flux. Two values are adopted, for the low and high magnetic field cases, respectively: $\chi_B = 10^{-3}$ and 1.

3   Results

We obtain the inverse Compton (IC) and synchrotron radiative output for different scenarios: the steady and flare stage, for low and high magnetic fields and different observing angles. This results are shown in Figs. 2 and 3. We focus on the $\phi = 30°$ case, being more representative of both Cyg X-3 and Cyg X-1, and specifically on the GeV band, resumed in Tab. 1.

Table 1: Values of the integrated emission in the 0.1 - 100 GeV band, given in erg s^{-1}, considering an observer angle of $\phi_{\mathrm{obs}} = 30°$.

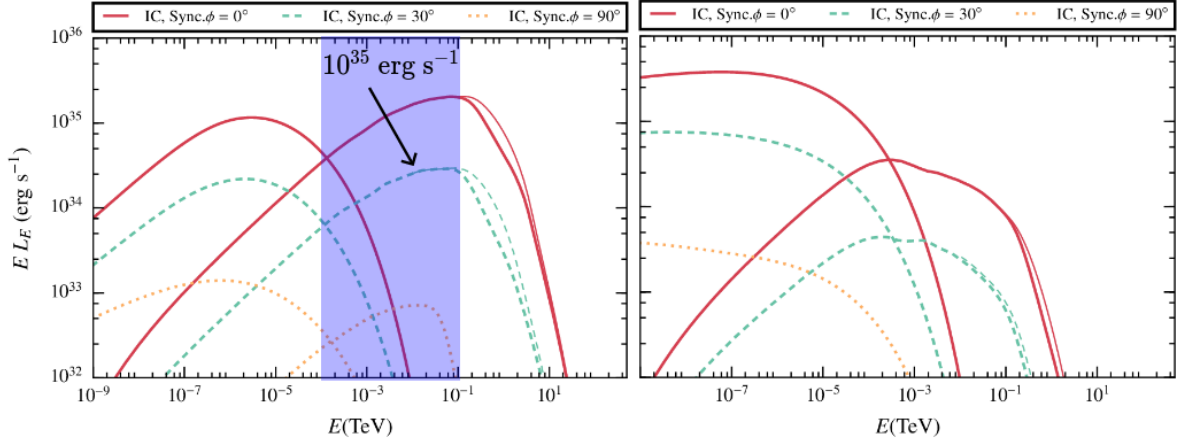| Stage	Low B ($\chi_B = 10^{-3}$)	High B ($\chi_B = 1$)
Steady	1.30×10^{35}	2.15×10^{34}
Flare	1.12×10^{36}	4.71×10^{34}

Figure 2: Spectral energy distributions (SEDs) for IC and synchrotron computed for the steady stage in the case of low magnetic field (left panel) and high magnetic field (right panel). The thin line in the IC curve corresponds to the emission that without taking into account absorption due to pair creation.
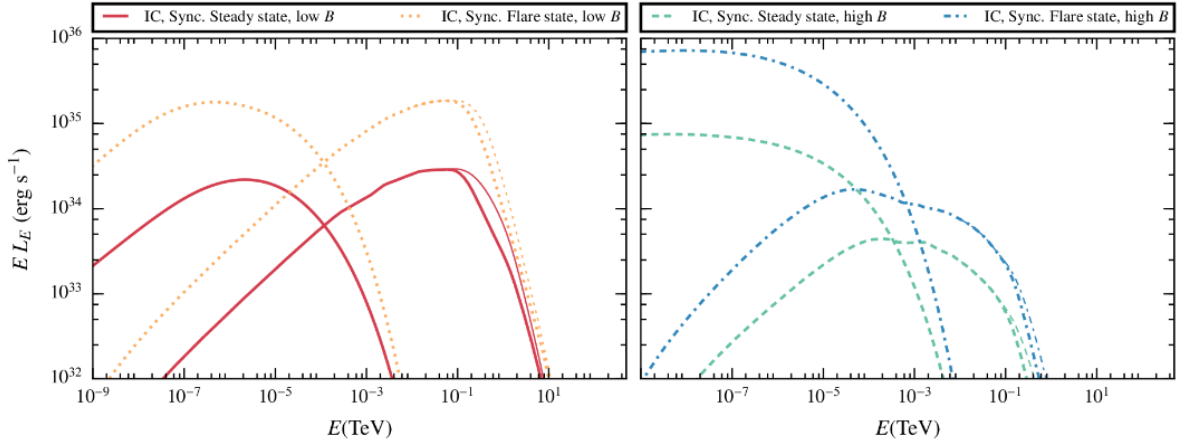

Figure 3: SEDs for the $\phi = 30°$ case for low (left panel) and high (right panel) magnetic fields, showing both stages: steady and flare.

4 Discussion

According to our results, for typical clumps with a size of a few % of the stellar size and a density ~ 10 times larger than the surrounding wind, they are able to penetrate the jet. The average number of such clumps inside the jet would be close to one at any time, and with reasonable non-thermal efficiencies our radiative results would be able to account for the luminosities observed in the GeV band for either Cyg X-3 and Cyg X-1. A more detailed study can be found in [5].

Acknowledgments

References

[1] Albert, J., Aliu, E., Anderhub, H., et al. 2007, ApJ, 665, L51

[2] Araudo, A. T., Bosch-Ramon, V., & Romero, G. E. 2009, A& A, 503, 673

[3] Bosch-Ramon, V. 2015, A& A, 575, A109

[4] de la Cita, V. M., Bosch-Ramon, V., Paredes-Fortuny, X., Khangulyan, D., & Perucho, M. 2016, A& A, 591, A15

[5] de la Cita, V. M., del Palacio, S., Bosch-Ramon, V., et al. 2016b, A& A, submitted

[6] Donat, R., Font, J. A., Ibez, J. M. l., & Marquina, A. 1998, Journal of Compu- tational Physics, 146, 58

[7] Donat, R. & Marquina, A. 1996, Journal of Computational Physics, 125, 42

[8] Moffat, A. F. J. 2008, in Clumping in Hot-Star Winds, ed. W.-R. Hamann, A. Feldmeier, & L. M. Oskinova, 17

[9] Owocki, S. P. & Cohen, D. H. 2006, ApJ, 648, 565

[10] Romero, G. E., Del Valle, M. V., & Orellana, M. 2010, A& A, 518, A12

[11] Romero, G. E., Torres, D. F., Kaufman Bernad, M. M., & Mirabel, I. F. 2003, A& A, 410, L1

[12] Tavani, M., Bulgarelli, A., Piano, G., et al. 2009, Nature, 462, 620

[13] Zanin, R., Fernndez-Barral, A., de Oa-Wilhelmi, E., et al. 2016, ArXiv e-prints